Large Dynamic Deformations of Beams, Rings, Plates, and Shells

EMMETT A. WITMER,* HANS A. BALMER,†
JOHN W. LEECH,‡ AND THEODORE H. H. PIAN§
Massachusetts Institute of Technology, Cambridge, Mass.

The axisymmetric responses of shells, plates, rings, and beams to impulsive or blast loading that produces large deformations involving both the elastic and plastic regions of material behavior are analyzed. A general numerical method that includes 1) elastic, 2) perfectly plastic, 3) elastic, strain-hardening, and/or 4) elastic, strain-hardening, strain-rate sensitive material behavior and large structural deflections has been formulated and applied. In the time-wise step-by-step numerical analysis, the increments in stress resultants and stress couples are determined by idealizing the shell thickness as consisting of n concentrated layers of materials separated by a material that cannot carry normal stresses but has infinite shear rigidity. The influences of the number of layers employed in the idealized model, as well as the forementioned various types of material behavior, are demonstrated. Theoretical predictions of time history responses and/or final structural deformations are compared with experimental data for impact-loaded spherical shells, for blast-loaded circular plates, and for explosively loaded circular rings and clamped beams.

Introduction

THIS paper presents the results of an initial attempt to develop a general method for predicting the response and permanent plastic deformation of shells under dynamic loading conditions.

Permanent plastic deformations of simple structures under high-intensity impulsive loadings have been analyzed by the so-called rigid-plastic analysis. In the case of simple beams, closed-form analytical solutions have been obtained.[1, 2] Applications to rings, curved beams, and circular plates also have been made.[3–5] In most cases, however, the solution of the resulting nonlinear differential equations still must rely on numerical methods.

The rigid-plastic analysis, strictly speaking, is applicable only to problems for which the initial kinetic energy is much higher than the elastic energy. This condition, of course, cannot be realized in most practical problems. Furthermore, recent investigations of beams have indicated appreciable discrepancies between rigid-plastic theory and experiments.[6] These discrepancies have been attributed largely to the effects of strain rate on the yield stress of the structural material. The rigid-plastic analysis is also in error for materials that exhibit appreciable strain-hardening in the plastic range. The existing dynamic analyses of rigid-plastic structures also are limited to cases involving small deflections. When large-deflection effects are taken into account, a rigid-plastic analysis becomes much too complicated; as a result, numerical analysis must be employed.

The present proposed method for dynamic analysis of shells is a general numerical method. It takes into account the effects of elastic-plastic or elastic-strain hardening behavior, strain rate, and large deflections.

In the following theoretical development, the analysis of two-dimensional structures such as beams and rings is described first. The analysis then is extended to the case of axisymmetric response of plates and shells with rotational symmetry. The accuracy of the numerical solutions then is evaluated by comparison with experimental results obtained for beams, rings, plates, and spherical shells under impulsive loadings.

Theoretical Formulation

Since the prediction of large degrees of dynamic structural response and permanent deformation is desired, the theoretical analysis must account for large deformations as well as elastic and inelastic material behavior. The present analysis, described in detail in Ref. 7, accounts for these effects but neglects the effects of rotary inertia and transverse shear deformations and is restricted accordingly. It will be seen that a forcing function of arbitrary distribution and time history can be accommodated readily.

Two-Dimensional Structures

Equations of motion

Figure 1 illustrates the internal and external forces acting upon a deformed element of length ds of a two-dimensional structure. The internal forces consist of moments, axial forces, and shear forces normal to the centroidal axis of the structure. The external forces may be considered to consist of inertia forces and forces externally applied normal and tangential to the exposed surfaces; these may be expressed in terms of convenient components.

The differential equations of dynamic equilibrium of this structural element in the y and z directions, respectively, are

$$(\partial/\partial s)(N\cos\theta) - (\partial/\partial s)(Q\sin\theta) + F_y - m\ddot{v} = 0 \quad (1)$$

$$(\partial/\partial s)(N\sin\theta) + (\partial/\partial s)(Q\cos\theta) + F_z - m\ddot{w} = 0 \quad (2)$$

Presented at the AIAA Launch and Space Vehicle Shell Structures Conference, Palm Springs, Calif., April 1–3, 1963. This research was sponsored by the Flight Dynamics Laboratory, Aeronautical Systems Division, U. S. Air Force, under Contract AF 33(657)-8427. The assistance and use of the facilities of the Massachusetts Institute of Technology Computation Center for part of the present calculations are acknowledged gratefully. The cooperation of Picatinny Arsenal and Aeronautical Systems Division personnel in furnishing needed data on the properties and responses of explosively loaded beams and circular rings is much appreciated.

* Associate Professor of Aeronautics and Astronautics. Associate Member AIAA.

† Senior Engineer, Aeroelastic and Structures Research Laboratory.

‡ Research Assistant, Department of Aeronautics and Astronautics. Associate Member AIAA.

§ Associate Professor of Aeronautics and Astronautics. Associate Fellow Member AIAA.

where $m = m(s)$ is the mass per unit length, θ is the slope of the structure $= \sin^{-1}(\partial w/\partial s)$, $(\dot{\ })$ denotes partial double differentiation with respect to time, and all other quantities are defined in Fig. 1.

The equation of moment equilibrium about an axis perpendicular to the yz plane is

$$(\partial M/\partial s) - Q = 0 \tag{3}$$

where rotary inertia has been neglected.

Equations corresponding to Eqs. (1–3) now will be written in finite-difference form. To do this it is convenient to consider the structure to be divided along its length into segments of initial length Δs_0. Let stations along the structure be designated as . . . s_{i-1}, $s_{i-1/2}$, s_i, $s_{i+1/2}$, s_{i+1}, etc., where the segment between stations $s_{i-1/2}$ and $s_{i+1/2}$ is termed the ith segment and has a length Δs_i. The mass of segment i is $m_i = m\Delta s_i$ and remains constant even if the length of the segment changes during the response due to straining along the axis of the structure. The dynamic equilibrium equation in the y direction for the ith segment can be written as

$$\frac{N_{i+1/2}\cos\theta_{i+1/2} - N_{i-1/2}\cos\theta_{i-1/2}}{\Delta s_i} - \frac{Q_{i+1/2}\sin\theta_{i+1/2} - Q_{i-1/2}\sin\theta_{i-1/2}}{\Delta s_i} + (F_y)_i - (m\ddot{v})_i = 0 \tag{4}$$

Multiplying through by Δs_i and setting $m\Delta s_i = m_i$, Eq. (4) becomes

$$N_{i+1/2}\cos\theta_{i+1/2} - N_{i-1/2}\cos\theta_{i-1/2} - Q_{i+1/2}\sin\theta_{i+1/2} + Q_{i-1/2}\sin\theta_{i-1/2} + (F_y)_i\Delta s_i - m_i\ddot{v}_i = 0 \tag{4a}$$

Similarly, the dynamic equilibrium equation for the ith segment in the z direction becomes

$$N_{i+1/2}\sin\theta_{i+1/2} - N_{i-1/2}\sin\theta_{i-1/2} + Q_{i+1/2}\cos\theta_{i+1/2} - Q_{i-1/2}\cos\theta_{i-1/2} + (F_z)_i\Delta s_i - m_i\ddot{w}_i = 0 \tag{5}$$

Similar equations could be written for any other segment or subsegment.

Corresponding to Eq. (3), the finite-difference moment equilibrium equation for the segment between stations $i - \frac{1}{2}$ and $i + \frac{1}{2}$ is

$$M_{i+1/2} - M_{i-1/2} - Q_i\,\Delta s_i = 0 \tag{6}$$

or, for the segment between stations i and $i + 1$,

$$M_{i+1} - M_i - Q_{i+1/2}\,\Delta s_{i+1/2} = 0 \tag{6a}$$

This moment equilibrium must hold, of course, for all segments and subsegments.

An inspection of the terms in Eqs. (4a, 5, and 6a), all of which must hold at all instants of time, indicates that these equations may be interpreted as describing a lumped-parameter model. This model is shown in Fig. 2 with quantities relabeled with whole rather than half indices for convenience. The model is seen to consist of concentrated masses connected by massless extensible links that remain straight between mass points; that is, for example, the axial forces acting on and between masses $i - 1$ and i both are inclined at an angle θ_i with respect to the horizontal. All bending is concentrated at the mass-point locations. The externally applied forces may be considered as being concentrated at each mass point, as shown.

For the relabeled lumped-parameter model shown in Fig. 2, the three previously discussed equilibrium equations are

$$N_{i+1}\cos\theta_{i+1} - N_i\cos\theta_i - Q_{i+1}\sin\theta_{i+1} + Q_i\sin\theta_i + F_{y_i}[(\Delta s_i + \Delta s_{i+1})/2] - m_i\ddot{v}_i = 0 \tag{7}$$

$$N_{i+1}\sin\theta_{i+1} - N_i\sin\theta_i + Q_{i+1}\cos\theta_{i+1} - Q_i\cos\theta_i + F_{z_i}[(\Delta s_i + \Delta s_{i+1})/2] - m_i\ddot{w}_i = 0 \tag{8}$$

$$M_i - M_{i-1} - Q_i\,\Delta s_i = 0 \tag{9}$$

In terms of the mass-point coordinates v, w, the link lengths

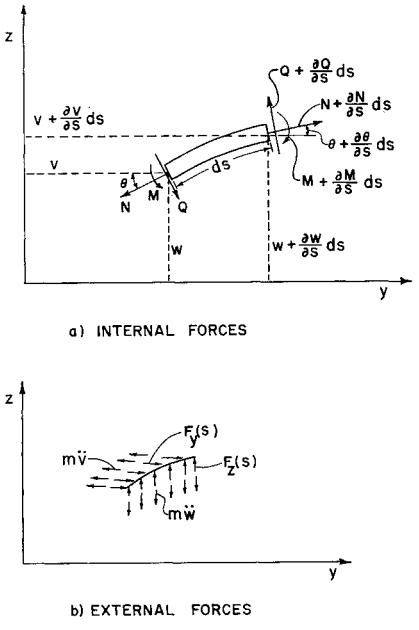

Fig. 1 Nomenclature for a two-dimensional structure.

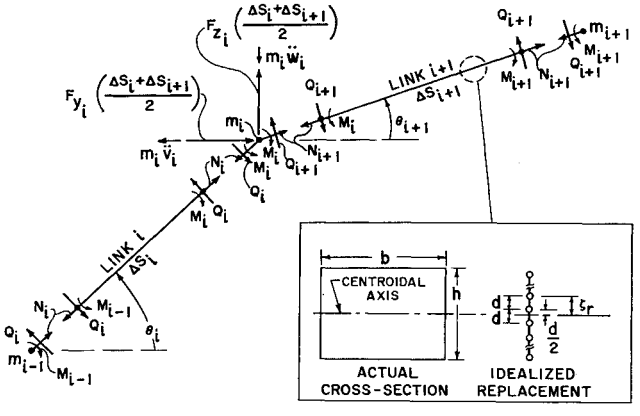

Fig. 2 Lumped-parameter and idealized-thickness model.

and angles may be written as

$$\Delta s_i = [(v_i - v_{i-1})^2 + (w_i - w_{i-1})^2]^{1/2} \tag{10}$$

$$\sin\theta_i = (w_i - w_{i-1})/\Delta s_i \tag{11}$$

$$\cos\theta_i = (v_i - v_{i-1})/\Delta s_i \tag{12}$$

The finite-difference equations (7–9), which approximate Eqs. (1–3), respectively, may be solved numerically for each mass point at successive instants of time j. Let it be assumed that, at time t_j, the following quantities already have been determined for all mass points of the structure: v_i, w_i, N_i, M_i, and ($\dot{v}_i$ and $\dot{w}_i$) if desired. Thus, Eqs. (10–12) can be used to calculate Δs_i, $\sin\theta_i$, and $\cos\theta_i$ for all links. Equation (9) then permits the determination of all Q_i. Then, if the F_y and F_z are given at time t_j, Eqs. (7) and (8) can be used to calculate $\ddot{v}_i$ and $\ddot{w}_i$ for all mass points at time t_j. Finally, since one may write, in general,

$$\ddot{x}_j = \frac{[(x_{j+1} - x_j)/\Delta t] - [(x_j - x_{j-1})/\Delta t]}{\Delta t} = \frac{x_{j+1} - 2x_j + x_{j-1}}{(\Delta t)^2} \tag{13}$$

the mass-point locations v_i and w_i at time $t_{j+1} = t_j + \Delta t$ may be written as

$$v_{i,j+1} = \ddot{v}_{i,j}(\Delta t)^2 + 2v_{i,j} - v_{i,j-1} \tag{14}$$

$$w_{i,j+1} = \ddot{w}_{i,j}(\Delta t)^2 + 2w_{i,j} - w_{i,j-1} \tag{15}$$

Having $v_{i,j+1}$ and $w_{i,j+1}$ for all points, one then can determine 1) the increment in strain along the axis of each link, and 2) the increment in the angles between neighboring links. From this information, one can determine the increments $\Delta N_{i,j+1}$ and $\Delta M_{i,j+1}$ or $N_{i,j+1}$ and $M_{i,j+1}$ for all links, and the calculation proceeds cyclically. Approximate determinations for these forces and moments are considered next.

Idealized-thickness model

Of a number of possibilities for determining the internal forces and moments in the present numerical method, the method explored herein consists of idealizing the actual structural cross section as consisting of n discrete, evenly spaced, equal-area layers of material that can carry normal stresses. These layers are considered to be separated by material that cannot carry normal stresses but that has infinite shear rigidity. With this simplified model (see Fig. 2), the stress and strain in the structure can be defined by the individual normal stresses in the n layers, invoking the assumption that plane sections remain plane throughout the response.

Considering, for the moment, structural material that is elastic-perfectly plastic, one might select the spacing between the discrete layers or areas and the size of the concentrated areas by requiring that the idealized model exhibit elastic extensional stiffness Ebh and elastic bending stiffness EI equal to those of the actual cross section of the two-dimensional structure. If the actual cross section were rectangular as shown in Fig. 2, requiring equal elastic extensional stiffness and taking equal Young's modulus leads to the following area A per "flange":

$$A = bh/n \tag{16}$$

Similarly, using equal Young's modulus and requiring equal elastic bending stiffnesses lead to the following spacings d between flanges:

$$d = h/(n^2 - 1)^{1/2} \tag{17}$$

If, on the other hand, one requires that the idealized model exhibit the same fully plastic pure axial load-carrying ability and equal fully plastic pure moment-carrying ability as the actual structure, the following flange areas and spacings result:

$$A = bh/n \tag{18}$$

$$d = h/n \tag{19}$$

It is seen that these two sets of conditions lead to the same flange areas, and flange spacings tend to approach each other as the number of flanges is increased.

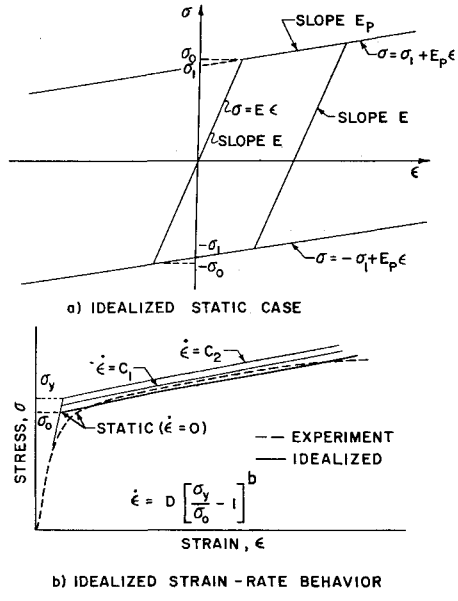

Fig. 3 Idealized stress-strain relations.

Strain-displacement relations

The strain in the rth flange located at a distance ζ_r (see Fig. 2) above the centroidal axis at mass point i may be expressed approximately as

$$\epsilon_i^r = \frac{\Delta s_i - \Delta s_{i,0}}{\Delta s_{i,0}} - \zeta_r \frac{\Delta\theta_i - \Delta\theta_{i,0}}{\frac{1}{2}(\Delta s_{i+1,0} + \Delta s_{i,0})} \tag{20}$$

where Δs_i is the length of the deformed link i, and $\Delta\theta_i$ is the angle between the deformed links i and $i + 1$. The index 0 refers to the undeformed position.

The first term in Eq. (20) is the axial strain in the ith link, and the second term represents the bending contribution evaluated at the ith mass point. For sufficiently small angles $\Delta\theta$, one may write

$$\Delta\theta_i \doteq \sin\Delta\theta_i = \sin(\theta_{i+1} - \theta_i) = \sin\theta_{i+1}\cos\theta_i - \cos\theta_{i+1}\sin\theta_i \tag{21}$$

thus relating the strains directly to the quantities given in Eqs. (10–12) which also are used in the subsequent equilibrium equations.

Strictly speaking, both terms in Eq. (20) should be evaluated at the same point. This could be done, for example, by averaging the axial strains of the links i and $i + 1$. For sufficiently small Δs, however, it is reasonable, alternatively, to use the axial strain in either of the neighboring links.

Having found the strains in all the flanges at time t_{j+1}, the strain increments can be determined by

$$\Delta\epsilon^r_{i,j+1} = \epsilon^r_{i,j+1} - \epsilon^r_{i,j} \tag{22}$$

and the associated flange stresses can be obtained from appropriate stress-strain relations. Once these stresses are found, the axial force and moment at each mass-point station may be computed from

$$N_{i,j+1} = A \sum_{k=-n/2}^{n/2} \sigma^k_{i,j+1} \tag{23}$$

$$M_{i,j+1} = A \sum_{k=-n/2}^{n/2} \sigma^k_{i,j+1}\,\zeta_k \tag{24}$$

where the idealized-thickness model is considered to consist of n flanges with areas concentrated at distances ζ_k from the centroidal axis.

Stress-strain relations

For the present discussion, let the engineering stress-strain behavior of the structural material be approximated as elastic, perfectly strain hardening as depicted in Fig. 3a. The allowable elastic paths all have slopes equal to Young's modulus E and are confined to the region lying between parallel lines of slope E_p intercepting the stress axis at $\pm\,\sigma_1$. For an elastic-perfectly plastic material, E_p would be zero.

With this idealization (or a suitable alternate), one can proceed to determine the stresses in each flange at each link and at each mass-point station. At time t_j, let it be assumed that the strain $\epsilon^k_{i,j}$ in each flange k at any given station i has been determined, and that the strain at time t_{j+1} also has been determined there as described earlier. Hence, the strain increment $\Delta\epsilon^k_{i,j+1}$ is known. The determination of the stress in a given flange and location at time t_{j+1} may be carried out systematically as follows in a numerical calculation:

1) Start by taking a trial value (superscript t) of σ_{j+1} computed by assuming an elastic path

$$\sigma^t_{j+1} = \sigma_j + E\,\Delta\epsilon_{j+1} \tag{25}$$

2) Check the sign of $\Delta\epsilon_{j+1}$ and proceed to see what the

correct value of σ_{j+1} must be:

$$\begin{aligned}
&\Delta\epsilon_{j+1} > 0 \begin{cases} \sigma^t_{j+1} > \sigma_1 + E_p\epsilon_{j+1} \rightarrow \sigma_{j+1} = \sigma_1 + E_p\epsilon_{j+1} \\ \sigma^t_{j+1} \leq \sigma_1 + E_p\epsilon_{j+1} \rightarrow \sigma_{j+1} = \sigma^t_{j+1} \end{cases} \\
&\Delta\epsilon_{j+1} = 0 \rightarrow \sigma_{j+1} = \sigma^t_{j+1} = \sigma_j \\
&\Delta\epsilon_{j+1} < 0 \begin{cases} \sigma^t_{j+1} \geq -\sigma_1 + E_p\epsilon_{j+1} \rightarrow \sigma_{j+1} = \sigma^t_{j+1} \\ \sigma^t_{j+1} < -\sigma_1 + E_p\epsilon_{j+1} \rightarrow \sigma_{j+1} = -\sigma_1 + E_p\epsilon_{j+1} \end{cases}
\end{aligned} \tag{26}$$

This procedure is applied separately to all flanges at each station. Having done this, the axial forces $N_{i,j+1}$ and moments $M_{i,j+1}$ can be determined from Eqs. (23) and (24), respectively. The cyclic timewise calculation of the dynamic response of the structure, as described in the paragraph following Eq. (12), then may proceed.

It should be remarked that rough approximations to the actual stress-strain curves may be adequate to permit reasonably accurate calculations of large dynamic structural deformations, provided that structural stability is not an important factor. Where instability (elastic or plastic) is an important factor, a much more accurate stress-strain representation is required for reliable results.[7] For such cases a Ramberg-Osgood-type representation, for example, is more appropriate.

For cases in which the structural material exhibits significant strain rate sensitivity, an approximate accounting for this effect may be made. Although numerous strain rate laws have been proposed and discussed, there appears to be no universally validated and accepted description. A convenient approximation previously employed by Ting,[8] among others, and used herein is shown in Fig. 3b. Here, the effect of strain rate is regarded as raising the yield point σ_y of the material above the static yield value σ_0, with the associated strain-hardening portion of the curve kept parallel to the static strain-hardening curve. The quantities D and b in the strain-rate expression shown are taken as constants of the structural material in question. In the numerical calculations, one readily can calculate the strain rate at any flange and location associated with the time interval from t_j to t_{j+1}, and, hence, an accounting for strain-rate effects may be accomplished readily.

The questions of appropriate 1) means for handling various boundary conditions, 2) space-mesh sizes, and 3) time intervals are discussed later.

Axisymmetric Shells

Equations of motion

Figure 4a shows a shell of revolution defined by the curvilinear coordinates s and φ. The location of any point on the meridian can be determined by the two coordinates r and z. On the element of the shell shown in Fig. 4b, there are two tangential stress resultants N_θ and N_φ, a transverse stress resultant Q_θ, and two stress couples M_θ and M_φ. The equations of equilibrium for large deflections of shells are

$$(\partial/\partial s)[N_\theta r\cos\theta] - (\partial/\partial s)[Q_\theta r\sin\theta] - N_\varphi - mr\ddot{r} = 0 \tag{27}$$

$$(\partial/\partial s)[N_\theta r\sin\theta] + (\partial/\partial s)[Q_\theta r\cos\theta] - mr\ddot{z} = 0 \tag{28}$$

$$[\partial(M_\theta r)/\partial s] - M_\varphi\cos\theta - Q_\theta r = 0 \tag{29}$$

where m is the mass of the shell per unit area, and θ is the angle of inclination of the element with respect to the r direction.

Equations corresponding to Eqs. (27–29) can be written in finite-difference form in the same manner as for the two-dimensional structures. These equations again can be interpreted as describing a lumped-parameter model consisting of rings connected by weightless frustums. The thickness of the shell also is idealized by n discrete layers of material that can carry normal stresses in the planes parallel to the tangential plane of the shell surface, whereas the material connecting these layers cannot carry normal stress but has infinite shear rigidity.

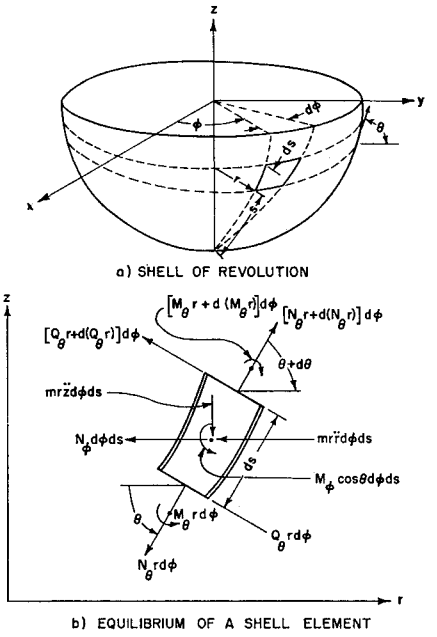

Fig. 4 Nomenclature for a shell of revolution.

Yield condition and flow rule

For each layer, the stress-strain relations under plane-stress conditions can be used. For example, for an elastic, perfectly plastic material, the Mises-Hencky yield condition[9] for the rth layer is given by

$$(\sigma_\varphi{}^r)^2 - (\sigma_\varphi{}^r)(\sigma_\theta{}^r) + (\sigma_\theta{}^r)^2 = \sigma_0{}^2 \tag{30}$$

where $\sigma_\varphi{}^r$ and $\sigma_\theta{}^r$ are the principal plane stresses, and σ_0 is the yield stress of the given material under uniaxial stress conditions.

The numerical procedure for solving the response of thin shells is similar to that for the two-dimensional structures. The increments in principal curvatures and midplane strains are expressed first in terms of the deflections in the r and z directions. The increments of total strains $\Delta\epsilon_\varphi$ and $\Delta\epsilon_\theta$ in each layer then can be determined by imposing the Kirchhoff's assumption that normals to the midsurface of the shell remain normal to the midsurface of the deformed shell. In the plastic range, these increments in strain must be resolved into their elastic and plastic components, i.e.,

$$\begin{aligned}
\Delta\epsilon_\varphi &= \Delta\epsilon_\varphi{}^e + \Delta\epsilon_\varphi{}^p \\
\Delta\epsilon_\theta &= \Delta\epsilon_\theta{}^e + \Delta\epsilon_\theta{}^p
\end{aligned} \tag{31}$$

where the elastic strain increments are given by

$$\begin{aligned}
\Delta\epsilon_\varphi{}^e &= (1/E)(\Delta\sigma_\varphi - \nu\Delta\sigma_\theta) \\
\Delta\epsilon_\theta{}^e &= (1/E)(\Delta\sigma_\theta - \nu\Delta\sigma_\varphi)
\end{aligned} \tag{32}$$

and the plastic strain increments can be written according to the incremental strain theory of plasticity, as follows:

$$\begin{aligned}
\Delta\epsilon_\varphi{}^p &= \tfrac{1}{3}(2\sigma_\varphi - \sigma_\theta)\Delta\lambda \\
\Delta\epsilon_\theta{}^p &= \tfrac{1}{3}(2\sigma_\theta - \sigma_\varphi)\Delta\lambda
\end{aligned} \tag{33}$$

where λ is a measure of the plastic deformation. Equation (31) thus contains three unknown quantities: $\Delta\sigma_\varphi$, $\Delta\sigma_\theta$, and $\Delta\lambda$. A third equation required for the solution is the yield condition:

$$\begin{aligned}
(\sigma_\varphi + \Delta\sigma_\varphi)^2 - (\sigma_\varphi + \Delta\sigma_\varphi)(\sigma_\theta + \Delta\sigma_\theta) + \\
(\sigma_\theta + \Delta\sigma_\theta)^2 = \sigma_0{}^2
\end{aligned} \tag{34}$$

Experiment

Several experiments that provide data against which to test predictions from the present numerical method are

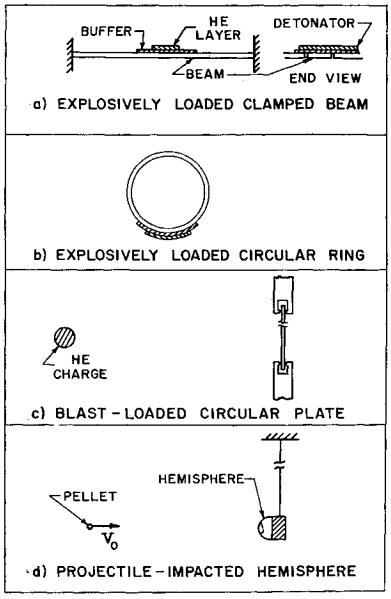

Fig. 5 Schematic of transiently loaded simple structures.

described briefly in the following. These include explosively loaded beams, explosively loaded circular rings, blast-loaded circular plates, and impact-loaded hemispheres. Each of these experiments is depicted schematically in Fig. 5.

Explosively Loaded Beams and Rings

Figure 5a illustrates schematically one type of experiment conducted recently at the Picatinny Arsenal which used clamped and simply supported rectangular beams of 6061-T6 and 2024-O aluminum alloy and heat-treated 1010 steel.[10] As indicated, the test specimen has its entire width and a portion of its span covered by a thin layer of high explosive (HE). The test specimen is separated from the HE layer by a suitable buffer material (in this case, polyethylene) that attenuates and lengthens the pressure pulse so that spall fracture of the test specimen by the otherwise excessively short-duration and intense pressure pulse produced by detonation of the thin layer of HE does not occur.

Through the use of high-speed streak and framing cameras, the deformation time history at the centerline of the span and the spanwise deformation at various times throughout the response to the permanent-deformation condition were obtained. Baffles were provided adjacent to the edges of the test specimen to reduce and/or prevent obscuration of the test specimen by the detonation products.

Since the duration of the pressure pulse applied to the beam from HE detonation is extremely short (i.e., typically less than about 5 μsec) compared with significant response times of the structure, the input may be treated as an impulse. In order to determine the impulse applied to the test specimens, an extensive calibration firing program was conducted in which "timepieces" of material identical in type, thickness, and width with that of the beams but having various spans in relation to the spanwise extent of the HE layer were used.[11] Various HE thicknesses were used; buffer material identical in type and thickness to that used in the beam tests also was used in the calibration experiments. Since these calibration specimens were suspended with essentially zero structural restraint, measurements by streak-camera and framing-camera photography of the velocities imparted to these specimens enable a determination of the imparted impulse to be made. Spanwise distribution effects arising from the finite span of the HE layer also were studied. Thus, well-defined inputs to the test specimens were obtained.

Similar experiments were conducted on freely suspended circular rings of 6061-T6 aluminum alloy (see Fig. 5b). The data on these dynamic response experiments available at this time include only inputs to and permanent deformations of the circular rings.[12] Further experiments of this type currently in progress will provide detailed deformation and strain time histories that can be used to test theoretical predictions.

Blast-Loaded Circular Plates

Reference 13 reports results of experiments in which 61S-T6 aluminum alloy flat plates, with uniform thicknesses of $\frac{1}{8}$, $\frac{1}{4}$, and $\frac{3}{8}$ in. and all having a 26-in. o.d. simply supported on a 24-in.-diam circle as shown schematically in Fig. 5c, were subjected to air blast from the detonation of spherical charges of pentolite of various weights placed on the axis normal to, through the center of, and at various distances from the circular flat-plate test specimen. The test frame in which the specimen was held extended laterally about 5 ft from the center of the plate to avoid undesirable edge effects upon the loading.

Only permanent deformation profiles for each test plate are reported. Response time histories apparently were not measured. Numerous measurements[14, 15] of blast characteristics permit a reasonable determination of the pressure time histories and/or impulse to which these plates were subjected.

Impact-Loaded Hemispheres

Reference 16 reports the results of experiments in which heat-treated 6061 aluminum alloy hemispherical shells were subjected to impact by a projectile. The test specimen was mounted on a fixture that, together with the test specimen, served as the bob of a ballistic pendulum and was impacted at its crown by a lead projectile of known mass and velocity (see Fig. 5d). Permanent deformations of the hemispherical shells were produced.

By applying the conditions expressing conservation of momentum and energy and by assuming that the energy of deformation of the projectile is negligibly small, the energy E_d, elastic and plastic, absorbed by the shell in reaching its final deformation can be obtained from ballistic pendulum measurements.[16] Detailed data on these experiments, including the permanent deformations produced and the associated values of E_d, are reported in Ref. 16. Two of these cases are discussed herein later.

Response Features and Comparison with Experiment

In this part of the paper, the application of the present numerical method to the prediction of dynamic large-deformation response of impulsively loaded beams and circular rings, blast-loaded flat circular plates, and impact-loaded hemispherical shells is described, and the results are compared with available experimental data. The effects of strain hardening, strain rate, number of layers in the idealized model, space-mesh size, and time interval on the dynamic large-deformation elastic-inelastic structural response are illustrated and/or discussed.

Impulsively Loaded Beams

The experimental data given in Ref. 10 pertain to both fixed and simply supported beams of 6061-T6 aluminum alloy, 2024-O aluminum alloy, and 1010 steel. A detailed analysis and correlation of these data with predictions using the present method may be found in Ref. 17. In the interests of clarity and conciseness, only the fixed-ended beams for these three materials are discussed here.

The 6061-T6 material was chosen as having essentially elastic-perfectly plastic behavior, the 2024-O as strongly strain hardening, and the 1010 steel as strongly rate sensitive. The beams had the following nominal dimensions: $\frac{1}{8}$- or $\frac{1}{4}$-in. thickness, 1.2-in. width, and 10-in. span between sup-

ports. HE with nominal thicknesses of 15 and 20 mils covered the entire width of each beam and was centered on the span covering a length from 1.0 to 2.0 in. As indicated in Fig. 5, the detonation front moved uniformly across the width direction of the beam; thus, strictly speaking, a pure two-dimensional response was not effected. Some twisting, as well as beam bending and stretching, was induced in each specimen. The twisting evident in the permanently deformed specimen was significant in some cases and very small in others.

The present predictions of dynamic response and permanent deformation pertain strictly to two-dimensional response. For analysis, the beam is represented as a lumped-mass model, as described with reference to Fig. 2 and as depicted schematically in Fig. 6. For calculation efficiency, the response was assumed to be symmetric about the midspan, although this is not necessary. The half-span was represented by 20, 30, and 40 masses with very little difference being observed in the predicted response for otherwise identical conditions. Therefore, 30 mass points per semispan were used for the remainder of the beam-response predictions discussed herein.

The cross section of the beam was represented by 2, 4, 6, and 10 concentrated-area layers of material in the thickness direction as described earlier. The time history of the vertical deflection at the semispan point of a representative impulsively loaded beam of elastic-perfectly plastic material is shown in Fig. 6, where the cross section of the beam is represented by 2, 4, and 10 layers; for this case the flange spacing d was taken as h/n, corresponding to fully plastic equivalence. It is seen that there are fairly distinct response differences between the two-flange and four-flange cases but insignificant differences between the four-flange and ten-flange cases. Similar degrees of comparison were noted at other spanwise stations.

Each mass point has freedom to move both vertically and horizontally in accordance with the forces to which it is subjected, except for the mass point adjacent to the fixed wall. This mass point is constrained by the computational procedure to move only horizontally in order to achieve the zero-deflection and zero-slope boundary conditions at the wall. Mass point 31 (imaginary) has been treated in two ways: 1) considered to be located as the mirror image of its neighbor on the other side of the wall, and 2) considered to be completely fixed. The resulting responses differ insignificantly; however, the former is believed to be physically the more realistic condition.

The time interval appearing in the finite-difference equations cannot be chosen arbitrarily. Exploratory calculations have been run for a typical case wherein various values of the ratio r have been taken between 0.2 and 0.96 with practically identical results. The quantity r is defined as

$$r = (\Delta t/\Delta s)(E/\rho)^{1/2} \tag{35}$$

where ρ is the mass density of the material. Divergence has been demonstrated when the ratio was chosen greater than one. In the calculations reported in the following, the ratio has been chosen to lie between 0.5 and 0.8.

The impulse input measurements reported in Ref. 11 indicate that a nearly uniform velocity is imparted to those portions of the test specimen immediately underneath the HE layer. For the region of the beam near the spanwise edges of the HE layer, a very steep gradient of imparted velocity is observed. These edge effects lead to a continuous distribution of imparted velocity extending beyond the HE-covered region and diminishing that which occurs within and near the edge of the HE-covered zone. It turns out that the total imparted impulse is essentially equal to that computed from strictly one-dimensional impulse calibrations, ignoring edge effects. Although a nonuniform impulse distribution can be taken into account in the present prediction method,[7] the present comparisons employed a uniform initial velocity

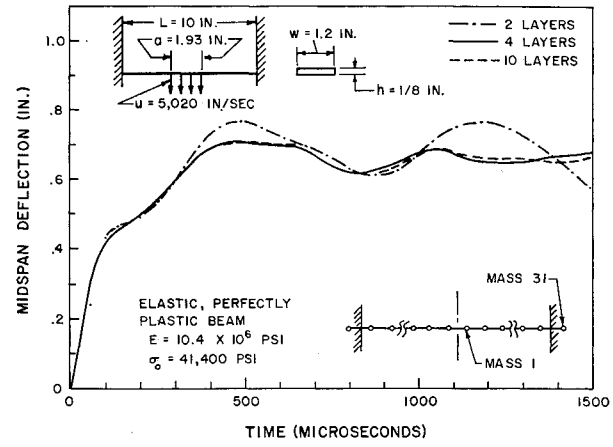

Fig. 6 Effect of number of layers of idealized model on beam dynamic response.

for that portion of the beam directly beneath the HE layer. This imparted velocity and the portion of the beam to which it pertains are indicated on each figure to be discussed.

Figure 7 presents a comparison of the measured midspan vertical deflection time history of an impulsively loaded 6061-T6 test specimen with the results of several calculations using the present numerical method. The calculation model employed 30 masses per semispan and six flanges for thickness idealization. The measured static stress-strain curves for several samples of the material used in the impulsive-loading tests were averaged and were approximated by two types of curve fits, each having in common an elastic part whose slope is equal to Young's modulus E of the material, 10.4×10^6 psi. In one fit, the material was approximated as being elastic-perfectly plastic with a yield stress $\sigma_0 = 41{,}400$ psi for the post-elastic range. In the second fit, the plastic range of the material was approximated by a straight line of slope $E_p = 76{,}100$ psi such that $\sigma_0 = 40{,}500$ psi and $\sigma_1 = 40{,}200$ psi (see Fig. 3). As an approximation for the effects of strain rate on the stress-strain properties, the strain rate formula of Fig. 3, with values of $D = 6500\ \text{sec}^{-1}$ and $b = 4$ given in Ref. 8, was employed.

For this 6061-T6 case, calculations were made for three material-behavior cases: 1) elastic-perfectly plastic (EL-PP), 2) elastic strain-hardening (EL-SH), and 3) elastic strain-hardening strain-rate (EL-SH-SR). Because of the very small differences between the results of cases 1 and 2 for this material, only cases 1 and 3 are shown in Fig. 7. It is seen that both the peak deformation and the permanent deformation predicted by case 1 are in reasonably good agreement with experiment. The differences between the pre-

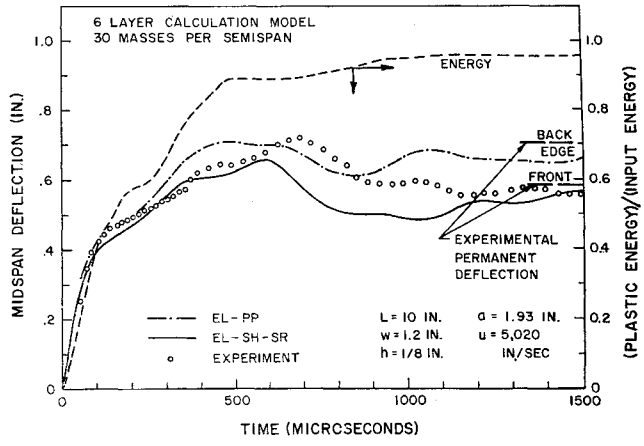

Fig. 7 Comparison of predicted and experimental responses of an explosively loaded clamped 6061-T6 beam.

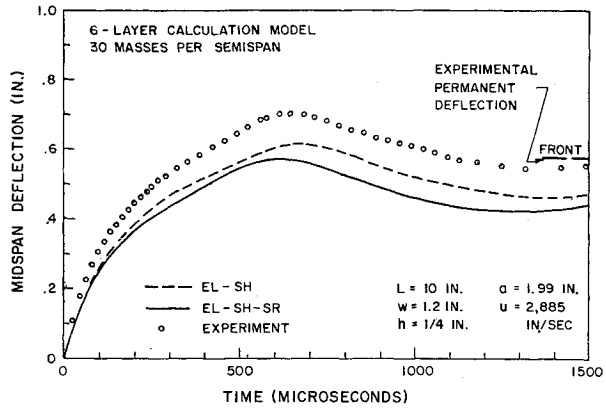

Fig. 8 Comparison of predicted and experimental responses of an explosively loaded clamped 2024-O beam.

dicted and observed response details may be an indication of improper accounting of the elastic behavior of the material throughout the response. Considering the EL-SH-SR calculations, it is seen that poorer agreement is achieved with respect to the value of the peak response, but the time at which this peak occurs is in better agreement with experiment than in the former comparison. Note also that the response details of the EL-SH-SR case are in better agreement with experiment. However, the experimental response shown is that of one edge of the beam, and this very well may include the effects of dynamic twisting, whereas the predictions are strictly for two-dimensional response. The measured midspan permanent deformations at each side of the beam also are shown in Fig. 7; this gives an indication of the probable permanent deflection of the centerline of the beam at midspan as well as the influence of twisting.

The present calculation permits an accounting for the time-wise and spanwise subsequent partitioning of the initially imparted kinetic energy to the specimen among plastic work, elastic energy, and kinetic energy of the system. To illustrate the time history of the energy absorbed by plastic work of the entire beam, the ratio of this energy to the initial imparted kinetic energy is shown in Fig. 7. For the structural excitation involved in this particular case, it is seen that about 89% of the total initially imparted kinetic energy has been absorbed by the time that the midspan deflection has reached its first peak. Later, about 95% of the initial input ultimately is converted to plastic work, with the remaining 5% alternating between elastic and kinetic forms. Ultimately this 5% also becomes dissipated by various mechanisms.

Figure 8 illustrates experimental-theoretical comparisons of the midspan vertical-deflection time history for a 2024-O aluminum alloy beam. The measured static stress-strain curve of the material was fitted with two straight lines, one

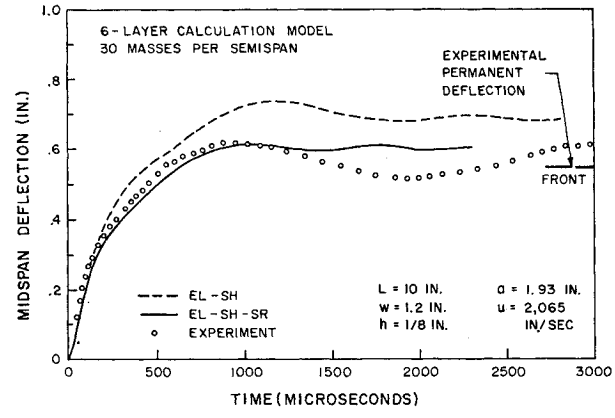

Fig. 9 Comparison of predicted and experimental responses of an explosively loaded clamped 1010 steel beam.

for the elastic region and one roughly approximating the plastic region up to about 4% strain. The associated quantities are $E = 10.4 \times 10^6$ psi, $\sigma_0 = 13{,}500$ psi, $\sigma_1 = 12{,}710$ psi, and $E_p = 606{,}000$ psi; this material exhibits considerably more strain-hardening than does the 6061-T6 material. As a qualitative comparison, the same strain-rate properties as used for the 6061-T6 material also were employed in the EL-SH-SR calculation for the 2024-O case.

From Fig. 8 it is seen that reasonably good experimental-theoretical agreement is obtained with respect to the times both to the first peak and to the first minimum. The general shapes of the predicted responses agree with experiment. However, the peak amplitudes are smaller than observed experimentally. Study is in progress to resolve this discrepancy. Here also a six-layer, 30-mass semispan calculation model was used.

The third material examined, 1010 steel, has been found to exhibit a considerable degree of static strain hardening. The static stress-strain curve for this material has been fitted with two straight lines: one for the elastic portion and a second roughly fitting the plastic region up to about 4%

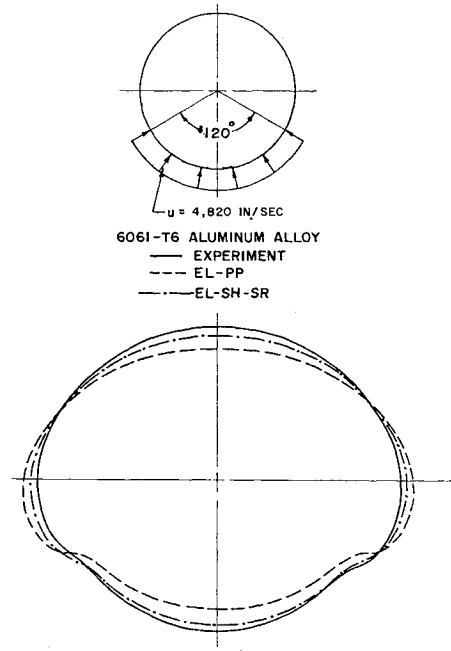

Fig. 10 Comparison of predicted with experimental permanent-deformation profile of an explosively loaded circular ring.

strain. The associated quantities are $E = 30 \times 10^6$ psi, $\sigma_0 = 11{,}600$ psi, $\sigma_1 = 11{,}450$ psi, and $E_p = 385{,}000$ psi. The strain rate data for mild steel reported in Ref. 8 were employed for the present comparisons: $D = 40.4$ sec^{-1} and $b = 5$.

Shown in Fig. 9 are comparisons of experiment for a 1010 steel example with predictions for EL-SH and EL-SH-SR cases using a six-flange, 30-mass semispan calculation model. Agreement between predictions and experiment is seen to be reasonably good with respect to both first peak and permanent midspan deflection. There remain some unexplained differences between the predicted and observed response time histories. Better material-property data from measurements currently in progress may help to resolve these differences.

Further comparisons between predicted and measured beam responses are given in Ref. 17. These include comparisons of strain time histories, spanwise deflections at a succession of instants of time, and improved representations of the mechanical stress-strain and strain-rate properties of the structural material, among others.

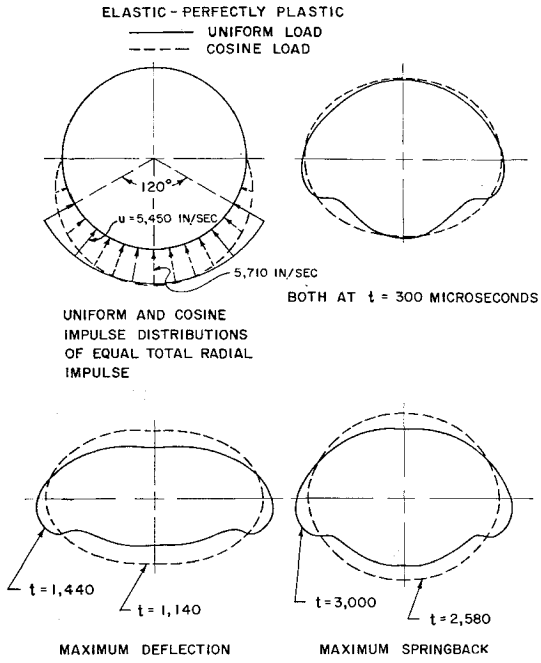

Fig. 11 Deformation response sequence of impulsively loaded circular rings (R = 3 in., h = 18 in., 6061-T6).

Impulsively Loaded Circular Rings

Preliminary experimental results[12] are available on the permanent deformation produced by impulsively loading freely suspended 6061-T6 aluminum alloy circular rings of 3-in. radius, $\frac{1}{8}$-in. thickness, and 1.2-in. width by detonating a layer of HE (suitably buffered) covering the full width of the ring and a peripheral sector of 120°. The permanent-deformation profile of a typical test specimen is shown in Fig. 10; this case corresponds to a total imparted radial impulse of 49.8×10^4 d-sec.

Treating the 6061-T6 material as EL-PP, with $E = 10.4 \times 10^6$ psi and $\sigma_0 = 41{,}400$ psi, and as EL-SH-SR, with $\sigma_0 = 40{,}500$ psi, $\sigma_1 = 40{,}200$ psi, $E_p = 76{,}100$ psi, $D = 6500$ sec^{-1}, and $b = 4$, the present numerical method was applied to the foregoing ring example. A six-flange-thickness model with 60 masses representing the complete ring was used in this case. Figure 10 shows the predicted permanent-deformation profiles of the ring. Although the data are preliminary, there is reasonably good qualitative and quantitative agreement between the predicted and the experimental permanent-deformation profiles.

A response prediction also has been made for a case identical to the foregoing except for a total imparted radial impulse of 56.5×10^4 d-sec. Figure 11 shows the predicted profile of the ring at several instants of time during the response, including the profiles corresponding to maximum central deflection and maximum springback. One striking but expected feature of the deformation response of this ring example is the existence of an inflection pattern of deformation produced by the discontinuous initial velocity distribution applied to the ring. This point of inflection appears to remain essentially stationary throughout the response of the ring. However, this may not be a general result. A significantly different deformation time history would be expected if the ring were subjected to a smooth distribution of initial velocity such as a cosine distribution.

To illustrate the nature of the deformation time history for a cosine initial-velocity distribution, a similar calculation was made in which the total radial impulse imparted to the ring was 56.5×10^4 d-sec. Otherwise, the calculation was identical. The results of this calculation also are shown in Fig. 11. For this input impulse, an inflection point in the deformation profile does not occur. However, it is expected

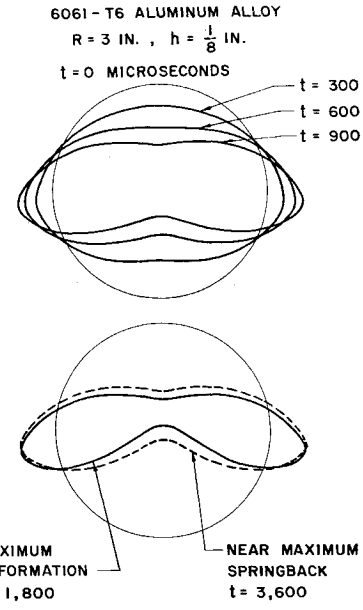

Fig. 12 Deformation response of a circular ring with a large cosine-distributed impulsive loading.

that, with a sufficiently intense impulse of cosine distribution, large-deformation profiles extending to and well beyond incipient "inflection-point" generation will be produced. This is illustrated in Fig. 12, where a sequence of deformation profiles is shown for a ring subjected to a more intense cosine distribution of imparted impulse, i.e., the total radial impulse imparted is 98.9×10^4 d-sec. These profiles indicate that the inflection point, in this case, moves from its point of initial appearance ($\theta \doteq 0°$) in the direction of increasing θ.

Blast-Loaded Simply Supported Circular Plates

For the case depicted in Fig. 5c, the axisymmetric analysis using the present numerical method was carried out treating the 61S-T6 aluminum alloy material as elastic-perfectly plastic. The lumped-parameter model employed is shown schematically in Fig. 13. The thickness of the plate has been idealized with a four-flange model. Preliminary calculations carried out using 20 and 32 masses to represent the radial length of the plate showed close response agreement. Hence, subsequent calculations employed a four-flange, 20-mass model.

The blast loading on the exposed 24-in. diam of the plate might be treated either as a uniformly applied impulse or as a time history of uniform loading. The plate response predicted on the basis of each of these inputs is shown in Fig. 13 for, respectively, $\frac{1}{8}$- and $\frac{3}{8}$-in.-thick plates subjected to blast from 8.35- and 36-lb charges of pentolite located on axis

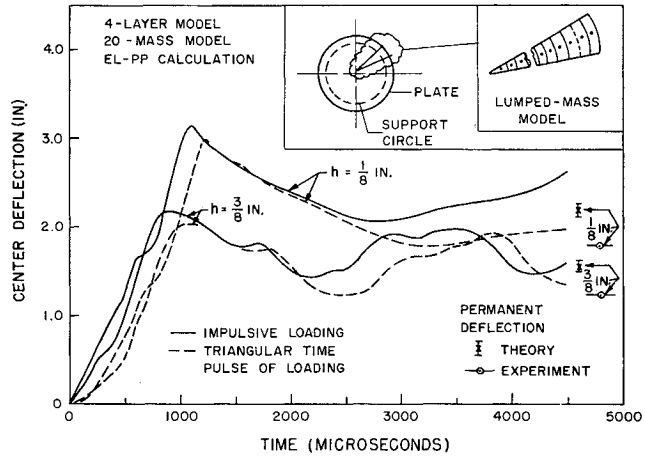

Fig. 13 Predicted blast-induced responses at the center of simply supported circular plates of 61S-T6.

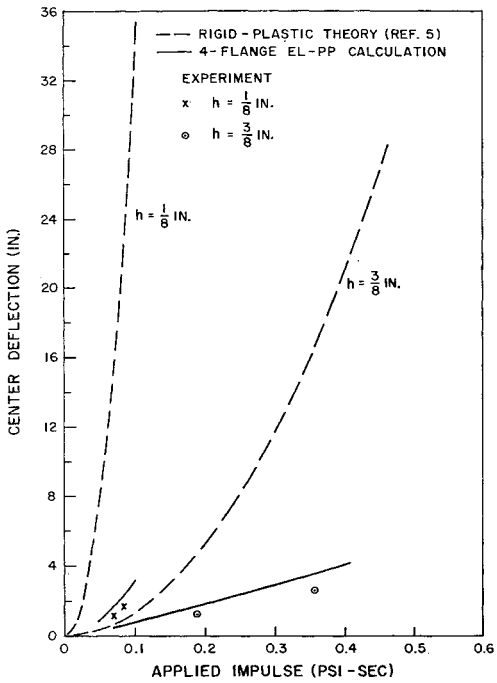

Fig. 14 Comparison of predicted permanent central deflection of simply supported blast-loaded circular 61S-T6 plates.

7.7 and 9.7 ft from the face of the plate. For these cases the respective applied impulse predicted from the data of Ref. 15 is 0.083 and 0.190 psi-sec; the same source indicates that the duration of the positive pressure loading is 1.32 and 1.43 msec. Also, the peak reflected shock overpressure; Δp_r is 283 and 615 psi. Although the pressure time history observed at such locations in many blast characteristics measurements[14, 15] can be well approximated by an exponential-type function decaying from an initial value equal to Δp_r, a simple triangular time history starting at Δp_r and reaching zero at a time such that the associated impulse is equal to the values already cited was used, for convenience, in the comparison shown in Fig. 13. The "theoretically correct" response time history is expected to lie somewhere between the two response curves of Fig. 13. The measured permanent central deformations also are shown in this figure.

A comparison of permanent deformations produced at the center of blast-loaded, flat-plate test specimens between experiment, rigid-plastic theory,[5, 13] and predictions from the present method is shown in Fig. 14. It is seen that the permanent deformation is vastly overpredicted by rigid-plastic theory. The permanent deformations predicted by the present calculation method are in better agreement but also are greater than those observed experimentally. The specific factors responsible for this overprediction have not been isolated and resolved yet. They may include, for example, inadequate representation of the stress-strain properties of the material, neglect of strain-rate effects, an inadequate representation of the flow process, uncertainties of the externally applied forces, etc. The experimental responses also may have exhibited asymmetries; this is implied but not reported explicitly in Ref. 13. Were this the case, however, the present axisymmetric theory would be expected to underpredict the permanent center deformation. Further study is needed to resolve these questions.

Impact-Loaded Hemispherical Shells

The hemispherical shells employed in these experiments had nominal 4-in. diam and uniform thicknesses ranging from 5 to 11 mils and were prepared by hydroforming, spinning, and chemical milling of 6061-O aluminum alloy. These

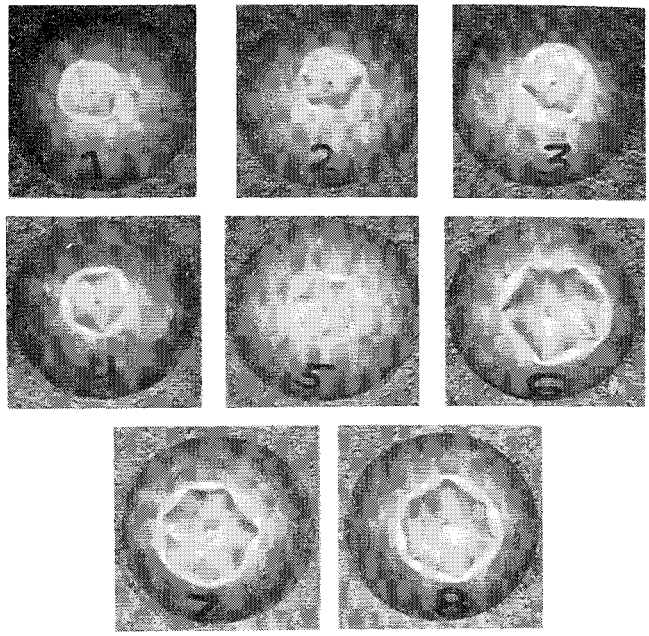

Fig. 15 Projectile-impacted hemispherical shells.

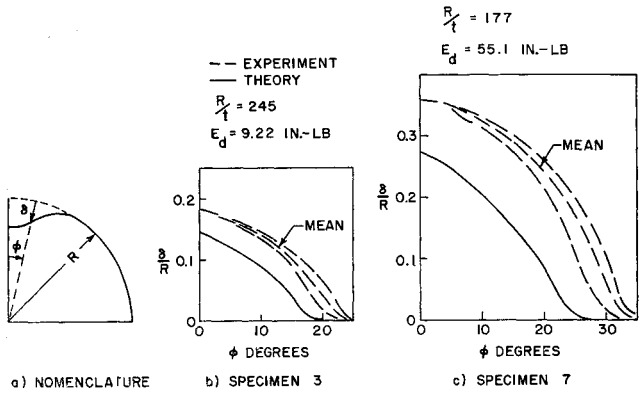

Fig. 16 Permanent-deformation profiles of projectile-impacted hemispherical shells.

models then were heat treated to a Rockwell hardness of 74 to 80, resulting in a compression yield of 36,000 psi for 0.2% offset and a tensile ultimate stress of 42,500 psi.

Photographs of eight impact-deformed hemispherical shells are shown in Fig. 15. The deformation patterns are seen not to be truly axisymmetric. This is illustrated also in Fig. 16, where the maximum, minimum, and mean deformation profiles measured along 10 directions across the impact-deformed region of each of two specimens are shown and reveal generally the extent of the asymmetry.

Predictions of the permanent deflections of models 3 and 7 were made using axisymmetric theory. In these calculations, the aluminum was treated as an elastic-perfectly plastic material with a yield stress of 39,000 psi. A two-layer idealized model with a flange separation of $h/2$ was used, where h is the actual thickness of the shell; this flange separation corresponds to that required for fully plastic equivalence. The resulting predicted permanent deflections are shown vs experiment in Fig. 16, where 30 segments per quadrant were employed in the calculation. Only very small differences in the results were found when 60 and 180 segments per quadrant were used.

It is seen that the permanent deformations predicted on the basis of the (highly restrictive) axisymmetric theory underestimate the experimental results by about 20%. From the asymmetric pattern of deformation actually observed, it is expected that larger central permanent deforma-

tions would be obtained from a given energy input than would occur from strictly axisymmetric deformation. Calculations in progress in which the axisymmetric restriction has been removed are expected to provide better agreement with experiment.

It is interesting to note, for example, that the present theory predicts that 97% of the input energy is absorbed by plastic work for shell specimen 7 (and this is completed by about 400 μsec after impact), with the remaining 3% being accounted for by elastic and kinetic energy of the shell.

Summary Comments

The matter of principal interest in the present study is the prediction of large dynamic elastic and post-elastic responses and permanent deformations of simple structures. The present formulation is restricted to two-dimensional and/or axisymmetric responses, neglecting the effects of shear deformation and rotary inertia. Approximate (straight-line EL-PP and EL-SH) representations of stress-strain properties of the structural material lead to reasonable theoretical-experimental agreement with peak response and permanent deformation. An approximate accounting for strain-rate properties of the material yields response time-history features agreeing better with experiment. Improvements in predictions are expected from the use of more accurate material property or constitutive data and more complete and faithful representations of those properties in the analysis.

The method outlined is simple and straightforward. This is because the displacement-strain, strain-stress, and equilibrium relations are solved sequentially, in this order, using a very short time interval. For example, it is easy to incorporate suitable constitutive relations since the strain increments are known at this stage of computation.

A number of features and comparisons such as spanwise deformation, strain, energy partitioning and distribution vs time, space-mesh size effects, other boundary conditions, etc., which space and time do not permit discussing here may be found in Ref. 17.

Note that the present two-dimensional, axisymmetric formulation requires the use of a small space mesh to permit reliable predictions of details of large dynamic response and permanent deformation, with the required space-mesh size depending upon the intensity, distribution, and time history of the forcing function. The resulting number of mass points and the required calculation time interval require considerable computing time even on an IBM 7090 type computer. Thus, it is desirable to use the present formulation as a learning tool to guide the formulation of simpler, less time-consuming prediction methods and to define realistically the conditions under which these (or other) simpler methods yield reliable predictions.

There are several obvious desirable extensions of the present formulation which can be cited and which currently are being carried out. One of the most important is the lifting of the two-dimensional and axisymmetric response restrictions; a more realistic theoretical-experimental comparison for the four types of experiments discussed herein then can be made. This step should be of particular importance in improving predictions of permanent deformations of projectile-impacted hemispherical shells and the incipient-buckling loading threshold for blast-loaded spherical shells.[18] Another interesting extension pertains to treating several geometric configurations of multilayer shells of similar or dissimilar materials bonded or unbonded between layers; within the restrictions of two-dimensional behavior, axisymmetric behavior, and the Kirchhoff assumption, this can be handled by the present formulation.

Further extensions to include ring-, frame-, and longeron-stiffened single- and multi-layer shells of various geometries would be helpful. A straightforward extension can be made, but the number of mass points involved and the computer time required to carry out a given response calculation would be formidable. Simplified, less time-consuming methods retaining the essential features of the problem should be sought; these will likely differ, for a given structure, depending upon the distribution, intensity, and time history of the forcing function.

References

[1] Symonds, P. S., "Large plastic deformations of beams under blast type loadings," Proc. 2nd U. S. Natl. Congr. Appl. Mech., 505–515 (1954).

[2] Pian, T. H. H., "A note on large plastic deformations of beams under transverse impact," Mass. Inst. Tech. ASRL TR 25-11 (May 1952).

[3] Owen, R. H. and Symonds, P. S., "Plastic deformations of a free ring under concentrated dynamic loading," J. Appl. Mech. **22**, 523–529 (1955).

[4] Chen, M. M., Hsu, P. T., and Pian, T. H. H., "Impulsive loading of rigid-plastic curved beams," Air Force Office Sci. Res. Rept. 316; also Proc. 4th U. S. Natl. Congr. Appl. Mech. **1**, 1039–1045 (1962).

[5] Wang, A. J., "Permanent deflection of a plastic plate under blast loading," J. Appl. Mech. **22**, 375–376 (1955).

[6] Bodner, S. and Symonds, P. S., "Experimental and theoretical investigation of the plastic deformations of cantilever beams subjected to impulsive loading," J. Appl. Mech. **29**, 719–728 (1962).

[7] Leech, J. W., Pian, T. H. H., Witmer, E. A., and Herrmann, W., "Dynamic response of shells to externally applied dynamic loads," Aeronaut. Systems Div. TDR-62-610 (July 1962).

[8] Ting, T. C. T., "The plastic deformation of a cantilever beam with strain rate sensitivity under impulsive loading," TR 70, Brown Univ., Contract Nonr-562(10) (July 1961).

[9] Nadai, A., *Theory of Flow and Fracture of Solids* (McGraw-Hill Book Co. Inc., New York, 1950), Chap. 16.

[10] Clark, E. N., Schmitt, F. H., and Ellington, D. G., "Explosive impulse on structures," Picatinny Arsenal, MIPR(33-616)61-31-no. 6 (September 30, 1962).

[11] Clark, E. N., Schmitt, F. H., and Ellington, D. G., "Explosive impulse on structures," Picatinny Arsenal, MIPR(33-616)61-31-no. 5 (June 30, 1962).

[12] Clark, E. N., private communication, Picatinny Arsenal, Dover, N. J. (February 1963).

[13] Hoffman, A. J., "The plastic response of circular plates to air blast," Master's Thesis, Univ. Delaware (June 1955).

[14] Hoffman, A. J. and Mills, S. N., "Air blast measurements about explosive charges at side-on and normal incidence," Boeing Research Labs. Rept. 988 (July 1956).

[15] Goodman, H. J., "Compiled free-air blast data on bare spherical pentolite," Boeing Research Labs. Rept. 1092 (February 1960).

[16] Witmer, E. A., Herrmann, W., Leech, J. W., and Pian, T. H. H., "Responses of plates and shells to intense external loads of short duration," Wright Air Dev. Div. TR 60-433 (April 1960).

[17] Balmer, H. A., Witmer, E. A., Leech, J. W., and Pian, T. H. H., "Theoretical-experimental correlation of large dynamic deformations of impulsively-loaded simple structures," Aeronaut. Systems Div. Tech. Doc. Rept. (in preparation).

[18] Witmer, E. A., Pian, T. H. H., and Balmer, H. A., "Dynamic deformation and buckling of spherical shells under blast and impact loading," *Collected Papers on Instability of Shell Structures*, NASA TN D-1510, pp. 607–622 (November 1962).